Iran University of Science and Technology

Automotive Science and Engineering

Journal Homepage: ase.iust.ac.ir

ISSN: 2008-9899

Differential Transformation Method for Vibration Analysis of Porous Functionally Graded Folded Plates

Davod Molaei[1], Mostafa Talebitooti[1*]

[1]Department of Mechanical Engineering, Qom University of Technology, Qom, Iran

ARTICLE INFO

Article history:
Received : 15 Nov 2024
Accepted: 29 Mar 2025
Published: 18 Apr 2025

Keywords:
Free Vibration
Folded Plate
Porosity
DTM

A B S T R A C T

This paper presents a novel investigation into the free vibration of porous folded plates using the differential transformation method (DTM). The porosity is functionally graded (FG) along the thickness of the plate, resulting in material properties that vary with the z-coordinate. The motion equations for each plate segment are derived based on classical plate theory (CPT), with simply-supported boundary conditions applied at the front edges, allowing the transformation of partial differential equations into ordinary differential equations. The differential transformation method is then employed to discretize the motion equations in the x-direction. By applying boundary conditions at the remaining edges and ensuring continuity at the joints, the eigenvalue problem is formulated, leading to the calculation of natural frequencies and mode shapes of the folded plate. The mathematical model is validated through comparisons with finite element method (FEM) results and existing literature. Results indicate that Type C porosity distributions exhibit the highest stiffness and resonant frequency compared to other porosity types. While frequency behavior is consistent across mode numbers regardless of porosity distribution and plate length, the impact of the porosity parameter on the frequency of Type C plates is demonstrably less significant than on other porosity types.

1. Introduction

Folded plates, characterized by their geometric efficiency and lightweight structure, are utilized extensively in a variety of applications, including roofs, automotive industry, bridges, and other structural systems. Understanding the vibrational behavior of these components is crucial, as they often experience dynamic loads that can lead to resonance, fatigue, and ultimately, structural failure. Analyzing their vibrational responses allows engineers to predict performance under various loading conditions, ensuring safety and longevity.

Numerous studies have investigated the behavior of folded plate structures using various methodologies, including finite element analysis [1-4], finite strip methods [5], step function [6], shear gap method [7] and generalized differential quadrature [8-10].

*Corresponding Author
Email Address: talebi@qut.ac.ir
https://doi.org/10.22068/ase.2025.699

[DOI: 10.22068/ase.2025.699]

In recent years, the use of porous plates in engineering structures has significantly increased. These materials facilitate improved drainage and aeration, making them advantageous for applications in civil engineering, environmental management, and mechanical systems. Furthermore, porous plates contribute to the durability and stability of structures by mitigating stress concentrations and distributing loads more evenly. Their incorporation can lead to increased efficiency and longevity of engineering projects, thus underscoring their significance in the design and implementation of modern infrastructure.

Hung et al. [11] have investigated the free vibration behavior of functionally graded porous plates reinforced with graphene platelets that exhibit magneto-electro-elastic properties (FGP-GPL-MEE). Shou et al. [12] have conducted a thorough analysis of the nonlinear dynamic response of stepped rectangular plates constructed from functionally graded porous material (FGPM) that are supported by a Kerr foundation within a thermal environment. Tayeb et al. [13] employed an analytical approach to investigate the free vibration behavior of porous functionally graded carbon nanotube-reinforced composite (FG-CNTRC) plates that are supported by elastic foundations. The carbon nanotube (CNT) reinforcement within the functionally graded plates is oriented randomly. The finite element method was initially employed by Thi [14] to model and analyze the free vibration and transient response of skew plates with non-uniform thickness, specifically bi-directional functionally graded sandwich porous (BFGSP) structures. Izadi et al. [15] have conducted a thorough analysis of the free vibrations of functionally graded porous (FGP) triangular plates of arbitrary shapes, incorporating elastic boundary conditions through the application of Isogeometric Analysis (IGA). For the first time, the free vibration of functionally graded graphene platelets reinforced porous composite (FG-GPLRPC) plate with multiple cutouts, including a rhombic hole, a teardrop-shaped hole and a crack have been investigated by zhang and Li [16]. Pham et al. [17] have undertaken a pioneering investigation that focuses on the free and forced vibration characteristics of functionally graded porous sandwich plates. These plates have been further enhanced through the incorporation of arbitrarily oriented stiffeners, which significantly contribute to their mechanical performance.

The literature review indicates that the vibration of porous folded plates has been primarily investigated using Finite Element Method (FEM) or other complex numerical techniques, which often entail significant implementation challenges. In this paper, we introduce the DTM for the first time as a means to analyze the free vibration of folded plates. This method is characterized by its straightforward implementation and the rapid convergence of results.

2. Theoretical Formulation

Figure 1(a) illustrates a porous folded plate, which is segmented into two flat portions for analytical purposes. Each segment employs a distinct local Cartesian coordinate system represented as (x_i, y_i, z_i) where i=1, 2. The dimensions of the first segment are L_1 and b, while the second segment measures L_2 and b. The fold angle is denoted by β. As demonstrated in Figure 1(b-d), the folded plate consists of porous aluminum foam with pore variations along the thickness direction. This study employs three types of pore distributions: uniform distribution (Type A), functionally graded distribution (Type B and C).

The three distinct porosity distribution patterns examined in this paper for the folded plate are illustrated in Fig. 1. These include a uniform porosity distribution (Type A) and two non-uniform symmetric patterns (Type B and Type C). Additionally, the elastic modulus of the functionally graded plate varies along the thickness direction as follows [18]:

$$\text{Type A: } E = (1 - e_A)E_0$$

$$\text{Type B: } E(z) = \left\{(1 - e_B\left[1 - cos\left(\frac{\pi z}{h}\right)\right])\right\}E_0$$

$$\text{Type C: } E(z) = \left\{(1 - e_C cos\left(\frac{\pi z}{h}\right)\right\}E_0 \qquad (1)$$

[DOI: 10.22068/ase.2025.699]

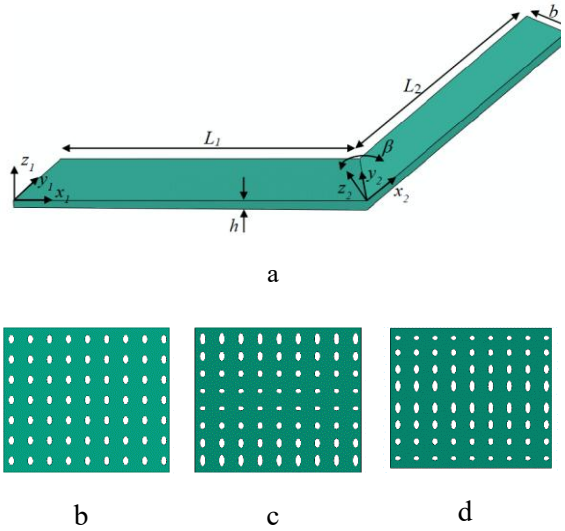

Figure 1: a) A depiction of a folded plate integrated with FG porous material and three types of porosity distribution along thickness, b)Type A, c)Type B and d)Type C

where E_0 represents the modulus of elasticity of the non-porous material, while e_A, e_B, and e_C denote for the porosity parameters.

To ensure a fair comparison of the porosity distribution patterns, it is advisable to standardize the porosity parameters to achieve equivalent mass values. This can be accomplished through the application of the equation relating density (ρ) to elastic modulus [19]:

$$\frac{E(z)}{E_0} = \left[\frac{\rho(z)}{\rho_0}\right]^{2.73} \tag{2}$$

The values of the porosity parameters e_A and e_B corresponding to specific values of the porosity parameter e_C are presented in Table 1, which can be summarized as follows.

$$e_A = 1.944\, e_c^6 - 3.417\, e_c^5 + 2.278\, e_c^4 - 0.6708\, e_c^3 + 0.122 e_c^2 + 0.6362 e_c$$

$$e_B = -0.4269\, e_c^3 - 0.009286\, e_c^2 + 1.732 e_c \tag{3}$$

To derive the motion equation of the plate based on Kirchhoff assumption, the in-plane displacement of plate *u* and *v* (parallel to the *x* and *y* axes) can be expressed as:

Table 1: Regulating the porosity parameters according to various distribution patterns

e_C	0	0.1	0.2	0.3	0.4	0.5
e_A	0	0.0640	0.1287	0.1942	0.2609	0.3988
e_B	0	0.1734	0.3426	0.5065	0.6637	0.9432

$$u = -z\frac{\partial w}{\partial x}$$

$$v = -z\frac{\partial w}{\partial y} \tag{4}$$

The linear strain-displacement relation are presented as follows:

$$\varepsilon_{xx} = \frac{\partial u}{\partial x},\ \ \varepsilon_{yy} = \frac{\partial v}{\partial y},\ \ \varepsilon_{xy} = \frac{\partial u}{\partial y} + \frac{\partial v}{\partial x} \tag{5}$$

The strains as a function of the out-of-plane displacement *w* can be derived by substituting (4) into (5).

$$\varepsilon_{xx} = -z\frac{\partial^2 w}{\partial x^2},\ \ \varepsilon_{yy} = -z\frac{\partial^2 w}{\partial y^2},\ \ \varepsilon_{xy} = -2z\frac{\partial^2 w}{\partial x \partial y} \tag{6}$$

According to the CPT, the plate is subjected to a condition of plane stress. Consequently, the stress-strain relationships can be articulated as follows:

$$\sigma_{xx} = \frac{E(z)}{1-\nu^2}\varepsilon_{xx} + \frac{\nu E(z)}{1-\nu^2}\varepsilon_{yy}$$

$$\sigma_{yy} = \frac{E(z)}{1-\nu^2}\varepsilon_{yy} + \frac{\nu E(z)}{1-\nu^2}\varepsilon_{xx}$$

$$\sigma_{xy} = G\varepsilon_{xy} \tag{7}$$

where *G* is the shear modulus and ν is Poisson's ratio which is assumed to be constant for porous material. As stated in a study by Zhang et al. [20], simplifying assumptions, including a constant Poisson's ratio, are often necessary to manage the complexity of analyzing FGPMs, particularly when focusing on the overall structural behavior.

By substituting (6) into (7) and integrating along the thickness direction, the resulting moments are derived as follows:

$$M_x = -D\left(\frac{\partial^2 w}{\partial x^2} + \nu\frac{\partial^2 w}{\partial y^2}\right)$$

[DOI: 10.22068/ase.2025.699]

$$M_y = -D\left(\frac{\partial^2 w}{\partial y^2} + \nu\frac{\partial^2 w}{\partial x^2}\right)$$

$$M_{xy} = M_{yx} = -(1-\nu)D\frac{\partial^2 w}{\partial x \partial y} \quad (8)$$

where D refers to flexural rigidity of the plate, defined as follows:

$$D = \int_{\frac{-h}{2}}^{\frac{h}{2}} \frac{E(z)z^2}{1-\nu^2} dz \quad (9)$$

Based on CPT, the shear forces in terms of moments are expressed as:

$$Q_x = \frac{\partial M_x}{\partial x} + \frac{\partial M_{xy}}{\partial y}$$

$$Q_y = \frac{\partial M_y}{\partial y} + \frac{\partial M_{xy}}{\partial x} \quad (10)$$

The utilization of (8) within (10) yields the following relationship.

$$Q_x = -D\frac{\partial}{\partial x}\left(\frac{\partial^2 w}{\partial x^2} + \frac{\partial^2 w}{\partial y^2}\right)$$

$$Q_y = -D\frac{\partial}{\partial y}\left(\frac{\partial^2 w}{\partial x^2} + \frac{\partial^2 w}{\partial y^2}\right) \quad (11)$$

By substituting (11) into dynamic equilibrium of forces in the z direction, the motion equation of plate are derived as:

$$D\left(\frac{\partial^4 w}{\partial x^4} + 2\frac{\partial^4 w}{\partial x^2 \partial y^2} + \frac{\partial^4 w}{\partial y^4}\right) + I\frac{\partial^2 w}{\partial t^2} = 0 \quad (12)$$

where I denotes the moment inertia, defined as follows:

$$I = \int_{\frac{-h}{2}}^{\frac{h}{2}} \rho(z) dz \quad (13)$$

Assuming simply-supported boundary conditions at the edges along the y-direction and a harmonic response with respect to time t, the transverse displacement of each segment of the folded plate, can be expressed as follows:

$$w_i(x, y, t) = \overline{w}_i\left(sin\frac{n\pi}{b}y\right)e^{i\omega t} \quad (14)$$

where ω is the natural frequency. By substituting (14) into (12), the partial differential equation (PDE) is reformulated as an ordinary differential equation (ODE) for each plate segment, expressed as follows:

$$D\left(\frac{d^4\overline{w}_i}{dx_i{}^4} - 2\frac{n\pi^2}{b^2}\frac{\partial^2\overline{w}_i}{dx_i{}^2} + \frac{n^4\pi^4}{b^4}\overline{w}_i\right) - I\omega^2\overline{w}_i = 0 \quad (15)$$

The motion equation for each segment is a fourth-order ordinary differential equation (ODE). Consequently, solving this equation necessitates two boundary conditions (BCs) along each edge parallel to the y-axis. Thus, by incorporating two BCs at $x_1 = 0$, two BCs at $x_2 = L_2$, and four continuity equations at the joint edge, a total of eight equations can be established, allowing for a feasible solution.

Boundary conditions at edges along y-axes:

Clamped (C): $w_i = 0, \quad \frac{\partial w_i}{\partial x_i} = 0 \quad (16)$

Simply-supported (Ss): $w_i = 0, \quad M_{x_i} = 0$ (17)

Free (F): $M_{x_i} = 0, \quad V_{x_i} = 0 = 0 \quad (18)$

where V_x is effective shear force, defined as follows:

$$V_x = Q_x + \frac{\partial M_{xy}}{\partial y} = -D\left[\frac{\partial^3 w}{\partial x^3} + (2-\upsilon)\frac{\partial^3 w}{\partial x \partial y^2}\right] \quad (19)$$

The continuity conditions at the joint edge of the folded plate can be expressed as follows:

$$w_1(L_1) = w_2(0)sin\left(\beta - \frac{\pi}{2}\right)$$

$$\frac{\partial w_1(L_1)}{\partial x_1} = \frac{\partial w_2(0)}{\partial x_2}$$

$$M_{x_1}(L_1) = M_{x_2}(0)$$

$$V_{x_1}(L_1) = -V_{x_2}(0)sin\left(\beta - \frac{\pi}{2}\right) \quad (20)$$

3. Differential Transformation method (DTM)

The Differential Transform Method (DTM) can be effectively employed to address vibration issues in folded plate. This method operates on the principle of converting ordinary and partial differential equations into algebraic equations. A concise overview of the methodology is outlined below.

According to the Taylor series expansion, the function $f(x)$ at the point $x = x_0$ can be expressed as:

[DOI: 10.22068/ase.2025.699]

$$f(x) = \sum_{r=0}^{\infty} \frac{(x-x_0)^r}{r!} \left[\frac{d^r f(x)}{dx^r}\right]_{x=x_0} \quad (21)$$

The rth-order differential transformation of a function $f(x)$ at the point $x = x_0$ can be defined as follows:

$$F[r] = \frac{1}{r!} \left[\frac{d^r f(x)}{dx^r}\right]_{x=x_0} \quad (22)$$

Thus, based on (21-22), the function $f(x)$ after the application of DTM about the point $x_0 = 0$ can be expressed as:

$$f(x) = \sum_{r=0}^{\infty} x^r F[r] \quad (23)$$

To address the vibration issues of folded plate through DTM, the governing differential equation, boundary condition equations, and continuity conditions are converted into a series of algebraic equations by applying transformation rules. The fundamental operations necessary for the differential transformation of the governing equations, boundary conditions, and continuity conditions are presented in Table 2.

Table 2: Basic operation of DTM

Original Functions	Transformed Functions
$f(x) = \alpha g(x)$	$F[r] = \alpha G[r]$
$f(x) = \frac{d^n g(x)}{dx^n}$	$F[r] = \frac{(r+n)!}{r!} G[r+n]$
$f(0) = 0$	$F[0] = 0$
$\frac{df(0)}{dx} = 0$	$F[1] = 0$
$\frac{d^2 f(0)}{dx^2} = 0$	$F[2] = 0$
$\frac{d^3 f(0)}{dx^3} = 0$	$F[3] = 0$
$f(L) = 0$	$\sum_{r=0}^{\infty} L^r F[r] = 0$
$\frac{df(L)}{dx} = 0$	$\sum_{r=0}^{\infty} rL^{(r-1)} F[r] = 0$
$\frac{d^2 f(L)}{dx^2} = 0$	$\sum_{r=0}^{\infty} r(r-1)L^{(r-2)} F[r] = 0$
$\frac{d^3 f(L)}{dx^3} = 0$	$\sum_{r=0}^{\infty} r(r-1)(r-2)L^{(r-3)} F[r] = 0$

By applying the DTM operation to (15), one can derive the recurrence equation in terms of r for the motion equations of each segment of the plate as follows:

$$W_i[r+4] = \frac{I\omega^2 - \frac{Dn^4\pi^4}{b^4}}{Dr(r+1)(r+2)(r+3)} W_i[r] + \frac{2n\pi^2}{b^2(r+2)(r+3)} W_i[r+2] \quad (24)$$

To illustrate the application of the DTM in free vibration analysis of folded plates, we consider an example involving a folded plate with clamped boundary conditions.

$$w_1(0) = 0 \xrightarrow{DTM} W_1[0] = 0$$
$$\frac{\partial w_1}{\partial x_1}(0) \xrightarrow{DTM} W_1[1] = 0 \quad (25)$$

Apply the DTM operation to two additional boundary conditions and four continuity equations; since the direct equation is not derived, we will consider the six relations as follows:

$$W_1[2] = c_1, W_1[3] = c_2, W_2[0] = c_3, W_2[1] = c_4, W_2[2] = c_5, W_2[3] = c_6 \quad (26)$$

The definition presented in (23) allows for the rephrasing of the remaining six boundary conditions (clamped) and continuity equations as follows:

$$w_2(L_2) = \sum_{r=0}^{\infty} {L_2}^r W_2[r] = W_2[0] + L_2 W_2[1] + {L_2}^2 W_2[2] + {L_2}^3 W_2[3] + {L_2}^4 W_2[4] + \cdots = 0$$

$$\frac{\partial w_2(L_2)}{\partial x_2} = \sum_{r=0}^{\infty} r{L_2}^{(r-1)} W_2[r] = W_2[1] + 2L_2 W_2[2] + 3{L_2}^2 W_2[3] + 4{L_2}^3 W_2[4] + \cdots = 0$$

$$w_1(L_1) - w_2(0)\sin\left(\beta - \frac{\pi}{2}\right) = \sum_{r=0}^{\infty} {L_1}^r W_1[r] - W_2[0]\sin\left(\beta - \frac{\pi}{2}\right) = W_1[0] + L_1 W_1[1] + {L_1}^2 W_1[2] + {L_1}^3 W_1[3] + {L_1}^4 W_1[4] + \cdots - W_2[0]\sin\left(\beta - \frac{\pi}{2}\right) = 0$$

[DOI: 10.22068/ase.2025.699]

$$\frac{\partial w_1(L_1)}{\partial x_1} - \frac{\partial w_2(0)}{\partial x_2} = \sum_{r=0}^{\infty} r{L_1}^{(r-1)} W_1[r] = W_1[1] + 2L_1 W_1[2] + 3{L_1}^2 W_1[3] + 4{L_1}^3 W_1[4] + \cdots - W_2[1] = 0$$

$$M_{x_1}(L_1) - M_{x_2}(0) = \frac{\partial^2 w_1(L_1)}{\partial {x_1}^2} - \frac{\nu n^2\pi^2}{b^2} w_1(L_1) - \frac{\partial^2 w_2}{\partial {x_2}^2}(0) + \frac{\nu n^2\pi^2}{b^2} w_2(0) = \sum_{r=0}^{\infty} r(r-1){L_1}^{(r-2)} W_1[r] - \frac{\nu n^2\pi^2}{b^2} \sum_{r=0}^{\infty} {L_1}^r W_1[r] - W_2[2] + \frac{\nu n^2\pi^2}{b^2} W_2[0] = 0$$

$$V_{x_1}(L_1) + V_{x_2}(0) sin\left(\beta - \frac{\pi}{2}\right) = \frac{\partial^3 w_1(L_1)}{\partial {x_1}^3} - (2-\nu)\frac{n^2\pi^2}{b^2}\frac{\partial w_1(L_1)}{\partial x_1} + \left[\frac{\partial^3 w_2}{\partial {x_2}^3}(0) - (2-\nu)\frac{n^2\pi^2}{b^2}\frac{\partial w_2(0)}{\partial x_2}\right] sin\left(\beta - \frac{\pi}{2}\right) = \sum_{r=0}^{\infty} r(r-1)(r-2){L_1}^{(r-3)} W_1[r] - (2-\nu)\frac{n^2\pi^2}{b^2} \sum_{r=0}^{\infty} r{L_1}^{(r-1)} W_1[r] + \left[W_2[3] - (2-\nu)\frac{n^2\pi^2}{b^2} W_2[2]\right] sin\left(\beta - \frac{\pi}{2}\right) = 0 \quad (27)$$

By substituting (24-26) into (27), we can rearrange the results into a matrix form:

$$\begin{bmatrix} a_{11} & a_{12} & a_{13} & a_{14} & a_{15} & a_{16} \\ a_{21} & a_{22} & a_{23} & a_{24} & a_{25} & a_{26} \\ a_{31} & a_{32} & a_{33} & a_{34} & a_{35} & a_{36} \\ a_{41} & a_{42} & a_{43} & a_{44} & a_{45} & a_{46} \\ a_{51} & a_{52} & a_{53} & a_{54} & a_{55} & a_{56} \\ a_{61} & a_{62} & a_{63} & a_{64} & a_{65} & a_{66} \end{bmatrix} \begin{Bmatrix} c_1 \\ c_2 \\ c_3 \\ c_4 \\ c_5 \\ c_6 \end{Bmatrix} = 0 \quad (28)$$

To achieve a non-trivial solution, the determinant of the coefficient matrix in (28) must be set to zero. For practical calculations, a finite number of terms must be used for each element of the matrix, ranging from 0 to R. Here, R signifies the upper limit of the summation operator. An optimal value for R can be established through convergence studies, which will be discussed in the subsequent section.

4. Results and discussion

To evaluate the convergence of the method, the natural frequencies for modes *m*=1 and *m*=2 under both clamped and simply-supported boundary conditions were obtained and summarized in Table 3. The results indicate that 30 terms are sufficient for convergence. Notably, the frequencies for the simply-supported condition converge more reliably than those for the clamped condition. It is due that a simply-supported allows for free rotation, implying a zero bending moment at the boundary. This condition translates to a simpler, often polynomial, expression within the DTM framework. In contrast, a clamped support restricts both displacement and rotation, necessitating a more complex representation within the DTM series.

Table 3: A convergence analysis of natural frequency (Hz) of folded plates ($\boldsymbol{L_1 = L_2 = 0.25m, b = 0.2m, h = 1mm, n = 1}$)

R	Clamped		Simply-supported	
	m=1	m=2	m=1	m=2
10	64.42	426.34	89.038	412.241
14	99.697	283.174	88.525	189.963
18	95.389	234.282	88.458	185.778
22	93.780	211.411	88.456	186.055
26	93.759	215.987	88.456	186.064
30	93.759	216.083	88.456	186.064
34	93.759	216.083	88.456	186.064

To validate the applied methodology and mathematical modeling, the present results are compared with findings from existing literature and those obtained using Abaqus software. Firstly, the current results for a flat plate (β = 180°) with fully simply supported boundary conditions are compared with the exact Navier solution, as detailed in Table 4. The second comparison involves the current results of the non-porous folded plate with β = 150° and those

[DOI: 10.22068/ase.2025.699]

obtained from the Abaqus software, as listed in Table 5. The slightly elevated frequency results obtained using the DTM compared to FEM for clamped boundary conditions are likely attributable to the inherent nature of the DTM approach. DTM relies on polynomial approximations and a finite order truncation, potentially leading to a stiffer representation of the system compared to the more versatile element formulations and refined discretization offered by FEA, particularly near the clamped edges where stress concentrations are significant. This increased stiffness results in a higher predicted natural frequency. In Figure 2, two mode shapes of folded plate with clamped boundary conditions obtained from Abaqus is illustrated.

Table 4: A comparative analysis of natural frequency (Hz) of fully simply-supported flat plates: present method versus exact solution ($L_1 = L_2 = 0.25m, b = 0.5m, h = 1mm$)

m	n=1		n=2		n=3	
	Exact	Present	Exact	Present	Exact	Present
1	24.402	24.402	61.005	61.005	122.009	122.009
2	61.005	61.005	97.608	97.608	158.612	158.612
3	122.009	122.009	158.612	158.612	219.617	219.617
4	207.416	207.416	244.019	244.019	305.023	305.023

Table 5: A comparative analysis of natural frequency (Hz) of clamped folded plates: present method versus exact solution ($L_1 = L_2 = 0.25m, h = 1mm, \beta = 150^o, b = 0.5m$)

n	m=1		m=2	
	Abaqus	Present	Abaqus	Present
1	85.68	85.70	257.55	257.62
2	116.87	116.93	289.87	289.99
3	173.24	173.32	345.50	345.71
4	255.40	255.52	425.62	425.92

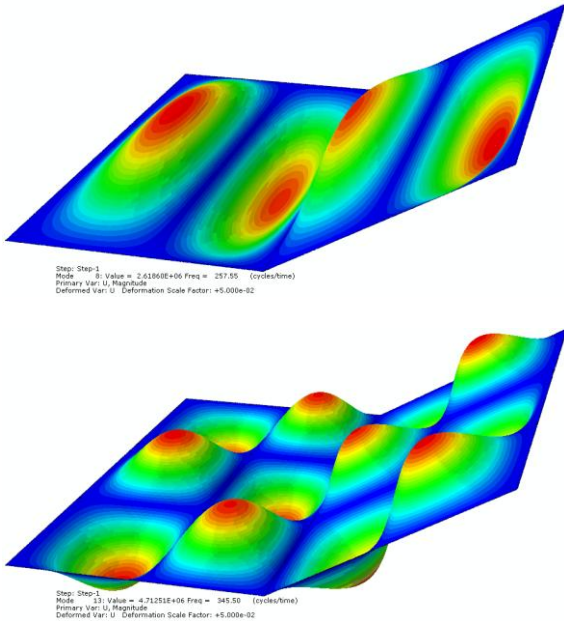

Figure 2: Two mode shapes obtained from Abaqus software

Thirdly, Table 6 presents a comparison study of the first three frequency parameters of GPLRC folded plates, contrasting the computed frequencies with those reported by Javani et al. [21] for fold angles of 60°, 90°, and 120°, under fully simply supported configurations. The discrepancy in frequency results between this study and the Generalized Differential Quadrature method (Ref. [21]), particularly in high modes and fold angle, may stem from the choice of basis functions. This work employs a Differential Transformation Method (DTM), which typically utilizes polynomials, whereas GDQ utilizes Legendre polynomials. Furthermore, the absence of information regarding the number of grid points used for the reference solution in Ref. [21] introduces another potential source of the observed differences. The outstanding alignment of the results demonstrates the accuracy of both the modeling and the methodology employed.

[DOI: 10.22068/ase.2025.699]

Table 6: First four frequency parameters $\Omega = \omega b\sqrt{\rho(1-\nu)/E}$ of fully simply-supported GPLRC folded plate ($\frac{b}{h} = 10, \frac{L_1}{b} = 0.5, \frac{L_2}{b} = 0.5$)

β		R	Ω_1	Ω_2	Ω_3
60°	Present	10	1.9451	7.4553	15.5544
		18	2.8802	4.0968	5.0439
		26	2.8310	3.7769	4.4532
		30	2.8310	3.7786	4.4561
		34	2.8310	3.7786	4.4576
	Ref. [21]		2.8315	3.7795	4.4589
90°	Present	10	2.0540	6.8880	16.1019
		18	3.0414	3.7851	5.2215
		26	2.9895	3.4895	4.6000
		30	2.9894	3.4911	4.6130
		34	2.9894	3.4911	4.6145
	Ref. [21]		3.0103	3.4992	4.6216
120°	Present	10	1.9746	6.5549	18.3068
		18	3.0013	3.3338	4.8129
		26	2.9293	3.0604	4.2209
		30	2.9296	3.0622	4.2243
		34	2.9296	3.0621	4.2257
	Ref. [21]		2.9400	3.0782	4.2780

The variation of the natural frequency of a folded plate with clamped edges along the y-direction in relation to the porosity parameter, e_c, for modes n=1 and n=2 is illustrated in Figure 3. The porosity parameters for Type A and Type B, as outlined in Table 1, are assumed to ensure that the mass of the plate remains constant. As illustrated in Figure 3, Type C exhibits the highest frequency, characterized by pores that varies from small at the outer surface to large at the mid-surface of the plate. Conversely, Type B displays the lowest frequency. Furthermore, the impact of the porosity parameter on the frequency of Type C is notably less pronounced than that observed in the other types. Concentrating pores in the center, as opposed to a uniform distribution or a distribution of holes on the outer surface, generally leads to a higher resonant frequency. This phenomenon arises from the interplay between stiffness and mass distribution within the structure. When pores are concentrated centrally, the outer regions of the structure retain greater material density and, consequently, higher stiffness. This stiffer outer layer acts as a constraint, effectively reducing the structure's overall flexibility. A stiffer structure inherently exhibits a higher natural frequency.

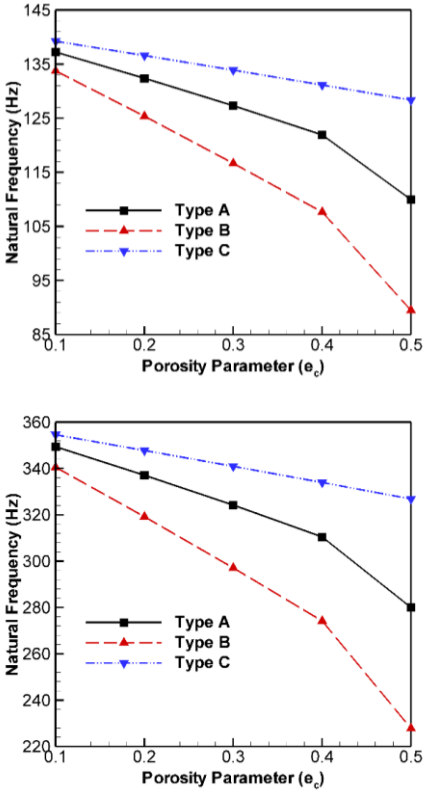

Figure 3: Variation of the natural frequency of clamped folded plates in relation to porosity parameters across various porous distributions, a)n=1 and b)n=2 ($\boldsymbol{L_1 = L_2 = 0.5\mathrm{m}, b = 0.2\mathrm{m}, h = 1mm, m = 1}$)

[DOI: 10.22068/ase.2025.699]

The relationship between the natural frequency of a folded porous plate and the length of its first segment, given that $L_1 + L_2$ remains constant, is depicted in Figure 4. The results indicate that as the length increases, the natural frequency decreases, although the rate of decline in frequency lessens over time. Although the total length of the sheet remains constant, the distribution of length between the two sections changes. The longer section (first section), due to its inherent reduced stiffness, dominates the overall stiffness of the folded system. In reality, the shorter section (second section) has greater stiffness, but the overall impact of the longer, less stiff section is greater. Additionally, the difference between the curves for varying lengths remains consistent, with Type C consistently exhibiting the highest frequency. The frequency behavior for both mode numbers, specifically n=1 and n=2, exhibits a notable similarity.

5. Conclusions

In this research, the vibration of a porous folded plate is investigated using the Differential Transform Method (DTM) for the first time. The implementation of DTM is detailed, and a summary of the results follows.

1- The convergence speed of the DTM is both rapid and reliable.
2- The porosity distribution classified as Type C exhibits the highest stiffness among various types, resulting in its corresponding frequency being the highest as well, presents a promising configuration for enhancing structural integrity in lightweight designs.
3- The frequency behavior in relation to porosity distribution and plate length remains consistent across different mode numbers and can be reliably applied in various design scenarios.
4- The influence of the porosity parameter on the frequency of Type C plates is less pronounced compared to other types which is beneficial in manufacturing and application.

In summary, leveraging Type C porosity distribution in folded plate designs can lead to stiffer, lighter, and more reliable automotive structures.

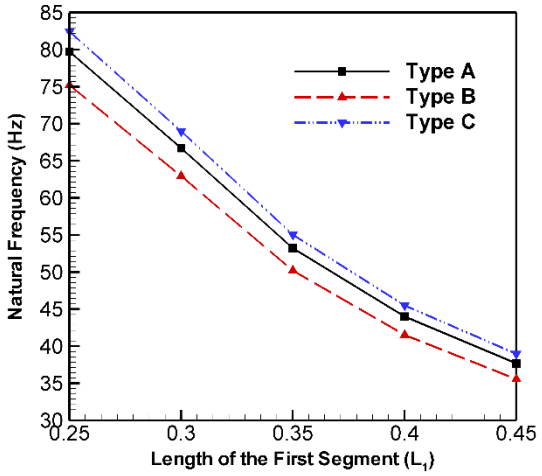

a

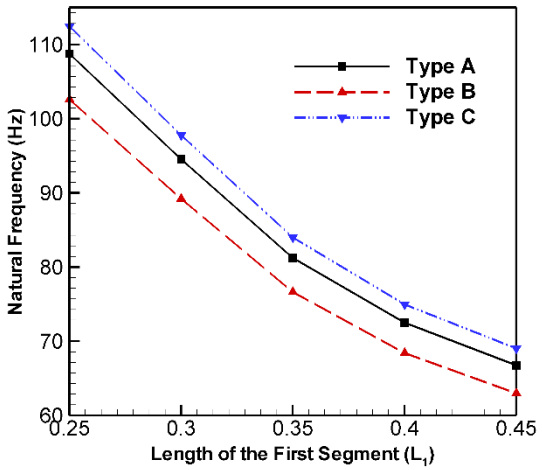

b

Figure 4: Variation of the natural frequency of clamped folded plates versus first segment length for various porous distributions, a)n=1 and b)n=2 $(\boldsymbol{L_1 + L_2 = 0.5\mathrm{m}, b = 0.2\mathrm{m}, h = 1mm, m = 1})$

Declaration of Conflicting Interests

The author(s) declared no potential conflicts of interest with respect to the research, authorship, and/or publication of this article.

[DOI: 10.22068/ase.2025.699]

References

[1] W.H. Liu, C.C. Huang, Vibration analysis of folded plates, Journal of Sound and Vibration, Volume 157, Issue 1, 1992, Pages 123-137.

[2] S. Haldar, A.H. Sheikh, Free vibration analysis of isotropic and composite folded plates using a shear flexible element, Finite Elements in Analysis and Design, Volume 42, Issue 3, 2005, Pages 208-226.

[3] Erwin Hernández, Luis Hervella-Nieto, Finite element approximation of free vibration of folded plates, Computer Methods in Applied Mechanics and Engineering, Volume 198, Issues 15–16, 2009, Pages 1360-1367.

[4] Quoc-Hoa Pham, Trung Thanh Tran, Phu-Cuong Nguyen, Free and forced vibration analyses of unsymmetrical functionally graded porous folded sandwich plates using MITC3 elements, Ain Shams Engineering Journal,

Volume 15, Issue 5, 2024, 102640.

[5] E. Hinton, M. Özakça, N.V.R. Rao, Free vibration analysis and shape optimization of variable thickness plates, prismatic folded plates and curved shells: Part 1: finite strip formulation, Journal of Sound and Vibration, Volume 181, Issue 4, 1995, Pages 553-566.

[6] Yuanming Lai, Wenbin Yu, Analytical solution for forced vibration of a simply-supported V-shaped folded plate roof, Thin-Walled Structures, Volume 40, Issue 3, 2002,

Pages 215-223.

[7] N. Nguyen-Minh, T. Nguyen-Thoi, T. Bui-Xuan, T. Vo-Duy, Static and free vibration analyses of stiffened folded plates using a cell-based smoothed discrete shear gap method (CS-FEM-DSG3), Applied Mathematics and Computation, Volume 266, 2015, Pages 212-234.

[8] Mehran Javani, Yaser Kiani, Mohammad Reza Eslami, On the free vibrations of FG-GPLRC folded plates using GDQE procedure, Composite Structures, Volume 286, 2022, 115273.

[9] Jijun Luo, Shengguang Peng, Suxia Hou, Yaser Kiani, Vibration analysis of FGM anisogrid lattice plates with one width fold based on the continuous model using the GDQE method, Thin-Walled Structures, Volume 195, 2024, 111386.

[10] Jing Zhang, Lianhe Li, Free vibration of functionally graded graphene platelets reinforced composite porous L-shaped folded plate, Engineering Structures, Volume 297, 2023, 116977.

[11] P.T. Hung, Chien H. Thai, P. Phung-Van, Isogeometric free vibration of functionally graded porous magneto-electro-elastic plate reinforced with graphene platelets resting on an elastic foundation, Computers & Mathematics with Applications, Volume 169, 2024, Pages 68-87.

[12] Haoge Shou, Vu Ngoc Viet Hoang, Peng Shi, Thermal vibration analysis of bi-directionally stepped porous functionally graded plates with segment-specific material property variation supported by Kerr foundation, Thin-Walled Structures, Volume 204, 2024, 112239.

[12] Haoge Shou, Vu Ngoc Viet Hoang, Peng Shi, Thermal vibration analysis of bi-directionally stepped porous functionally graded plates with segment-specific material property variation supported by Kerr foundation, Thin-Walled Structures, Volume 204, 2024, 112239.

[13] Tayeb SI TAYEB, Mohammad Amir, Sang-Woo Kim, Dongkuk Choi, An analytical modelling of free vibration in porous FG-CNTRC plate resting on elastic foundations, Materials Today Communications, Volume 40, 2024, 109925.

[14] Hong Nguyen Thi, Finite element approach for free vibration and transient response of bi-directional functionally graded sandwich porous skew-plates with variable thickness subjected to blast load, Defence Technology, Volume 42, 2024, Pages 83-104.

[15] Milad Izadi, Maryam Abedi, Paolo S. Valvo, Free vibration analysis of a functionally graded porous triangular plate with arbitrary shape and elastic boundary conditions using an isogeometric approach, Thin-Walled Structures, Volume 205, Part B, 2024, 112422.

[DOI: 10.22068/ase.2025.699]

[16] Jing Zhang, Lianhe Li, Free vibration of functionally graded graphene platelets reinforced porous composite plate with multiple cutouts, Thin-Walled Structures, Volume 209, 2025, 112952.

[17] Thanh-Tung Pham, Huu-Quoc Tran, Van-Long Nguyen, Kha-Hoa Le, Minh-Tu Tran, Free and forced vibration of functionally graded porous sandwich plates reinforced by arbitrarily oblique stiffeners, Thin-Walled Structures, Volume 210, 2025, 113039.

[18] Khorshidvand, Ahmad Reza, and Ali Reza Damercheloo. 2021. "Bending, Axial Buckling and Shear Buckling Analyses of FG-Porous Plates Based on a Refined Plate Theory." Australian Journal of Mechanical Engineering 21 (2): 705–24

[19] Yan Qing Wang, Zhi Yuan Zhang, Bending and buckling of three-dimensional graphene foam plates, Results in Physics, Volume 13, 2019, 102136.

[20] Yantao Zhang, Guoyong Jin, Mingfei Chen, Tiangui Ye, Chuanmeng Yang, Yaowei Yin, Free vibration and damping analysis of porous functionally graded sandwich plates with a viscoelastic core, Composite Structures, Volume 244, 2020, 112298.

[21] Mehran Javani, Yaser Kiani, Mohammad Reza Eslami, On the free vibrations of FG-GPLRC folded plates using GDQE procedure, Composite Structures, Volume 286, 2022, 115273.

[DOI: 10.22068/ase.2025.699]